Deterministic magnetization switching using lateral spin-orbit torque

Yi Cao[†], Yu Sheng[†], Kevin William Edmonds, Yang Ji, Houzhi Zheng, and Kaiyou Wang[*]

Dr. Y. Cao, Y. Sheng, Prof. Y. Ji, Prof. H. Zheng, Prof. K. Wang
State Key Laboratory for Superlattices and Microstructures
Institute of Semiconductors
Chinese Academy of Sciences
Beijing 100083, China
E-mail: kywang@semi.ac.cn

Dr. Y. Cao, Prof. K. Wang
Beijing Academy of Quantum Information Sciences
Beijing 100193, China

Dr. K. W. Edmonds
School of Physics and Astronomy
University of Nottingham
Nottingham NG7 2RD, United Kingdom

Prof. Y. Ji, Prof. H. Zheng, Prof. K. Wang
Center of Materials Science and Optoelectronic Engineering
University of Chinese Academy of Science
Beijing 100049, China

Prof. K. Wang
Center for Excellence in Topological Quantum Computation
University of Chinese Academy of Science
Beijing 100049, China

[†]These authors contributed equally to this work;
[*]Corresponding e-mail: kywang@semi.ac.cn

Keywords: lateral spin-orbit torque (Lateral SOT), localized laser annealing, lateral Pt/Co interface, current-induced magnetization switching.

Current-induced magnetization switching by spin-orbit torque (SOT) holds considerable promise for next generation ultralow-power memory and logic applications. In most cases, generation of spin-orbit torques has relied on an external injection of out-of-plane spin currents into the magnetic layer, while an external magnetic field along the electric current direction is generally required for realizing deterministic switching by SOT. Here, we report deterministic current-induced SOT full magnetization switching by lateral spin-orbit torque in zero external magnetic field. The Pt/Co/Pt magnetic structure was locally annealed by a laser track along the in-plane current direction, resulting in a lateral Pt gradient within the ferromagnetic layer, as confirmed by microstructure and chemical composition analysis. In zero magnetic field, the direction of the deterministic current-induced magnetization switching depends on the location of the laser track, but shows no dependence on the net polarization of external out-of-plane spin currents. From the behavior under external magnetic fields, we identify two independent mechanisms giving rise to SOT, i.e. the lateral Pt-Co asymmetry as well as out-of-plane injected spin currents, where the polarization and the magnitude of the SOT in the former case depends on the relative location and the laser power of the annealing track. Our results demonstrate an efficient field-free deterministic full magnetization

switching scheme, without requiring out-of-plane spin current injection or complex external stack structures.

For more than a decade, the electrical switching of ferromagnets (FM) with perpendicular magnetic anisotropy (PMA), using spin-transfer torque (STT) and more recently spin-orbit torque (SOT), has underpinned the development of fast, low-power-consumption, and high-density spintronic devices[1-5]. In general, both the STT- and the SOT-induced switching of a FM layer require an injection of out-of-plane spin current from nearby layers[6-8]. For STT-induced FM switching, particularly, a spin-polarized current is generated in a magnetic tunneling junction (MTJ) structure when a charge current flows perpendicularly through the stacks, where another FM layer acts as a spin-polarizer[9]. Thus, device instability issues arise since the tunneling barrier layer between the two FM layers is required to transmit large switching currents.

The SOT-induced FM switching, on the other hand, circumvents this problem by using an in-plane switching current. Conventionally, a stack structure consisting of a strong spin-orbit coupling (SOC) layer and a FM layer is used, where an in-plane charge current gives rise to an out-of-plane pure spin current due to spin Hall effect (SHE) in the SOC layer and/or Rashba effect from the perpendicular interfacial inversion asymmetry[10-13]. The resulting SOT-induced effective magnetic field is in-plane, hence an additional orthogonal in-plane magnetic field is required to realize deterministic switching of a PMA-FM. To date, several approaches for field-free SOT-induced PMA-FM switching have been proposed and

demonstrated, such as switching using a polarized ferroelectric substrate-induced in-plane spin current gradient[14-16], a wedge oxide capping layer[17], a tilted PMA layer[18], a stack with coherent in-plane exchange field[19-23], an interplay of SOT and STT[24,25], an in-plane-FM/normal metal/ PMA-FM trilayer[26], and a particular low symmetric WTe_2 semi-metal[27]. However, the concomitant complexities of these approaches highlight the inherent limitation of the conventional SOT scheme utilizing external out-of-plane spin current injection in a perpendicular asymmetric structure.

Here we demonstrate magnetic field-free deterministic current-induced magnetization switching in a PMA Pt/Co/Pt trilayer subjected to local laser annealing. Without external magnetic field, the direction of current-induced magnetization switching is found to depend on the relative location and the laser power of the annealing track, but is independent of the net spin current orientation from the two Pt layers. We attribute the observed behavior to a new SOT-induced perpendicular effective magnetic field originating from a lateral Pt gradient inside the Co layer. These results add further understanding to the physics of SOT and suggest a new scheme for magnetic field-free deterministic current-induced switching of a PMA-FM with more simplified stacks, even in the absence of out-of-plane spin current injections from neighbouring strong SOC layers.

Engineering current-induced FM switching by laser annealing

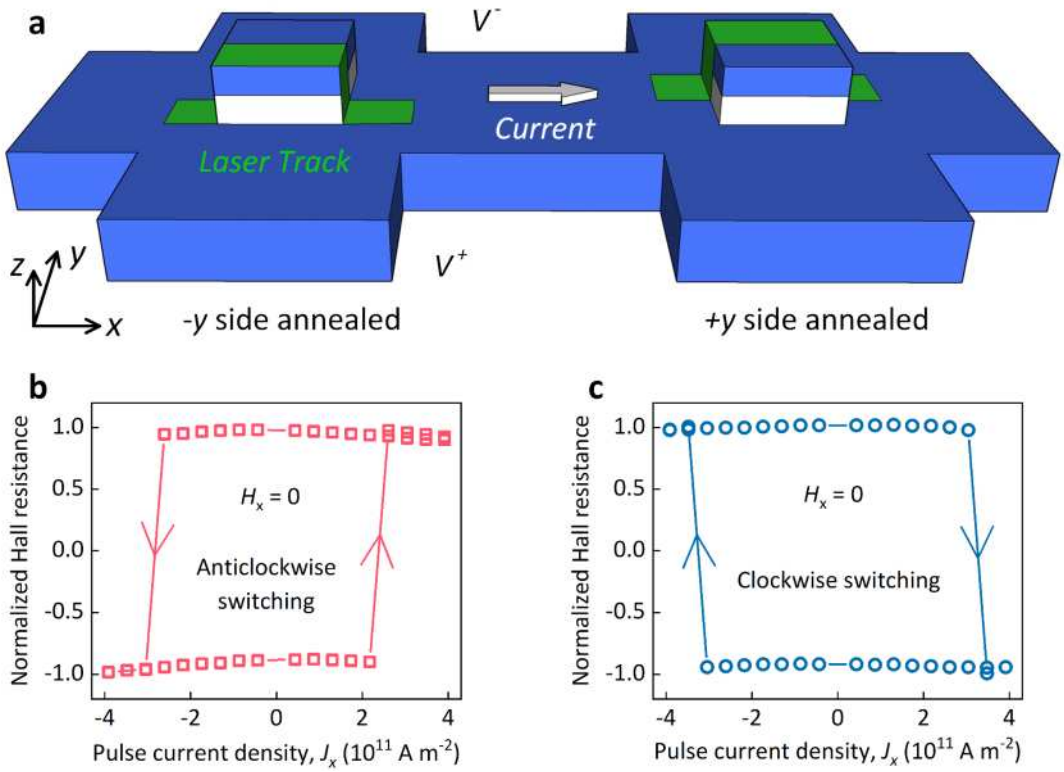

Figure 1 | Schematic drawing of the locally laser annealed PMA-FM pillars and the respective current-induced magnetization switching. a, Schematic of the Hall device with a stack structure of Pt(3)/Co(0.5)/Pt(2), where the top Co(0.5)/Pt(2) layers were fabricated into square pillars at each Hall cross. The Hall bar channel width and the pillar side length are 6μm and 2μm, respectively. Black arrows indicate the Cartesian (x, y, z) coordinate systems. Green zones illustrate the localized annealing tracks produced by an 8 mW laser, where the left/right device is annealed at the -y/+y side of the square pillar. **b-c**, In-plane (x-direction) pulse current induced perpendicular magnetization switching (represented by the normalized R_H-J_x loops) without external magnetic field for (**b**) the -y side annealed pillar and (**c**) the +y side annealed pillar, respectively. The current

density J_x was obtained by dividing the current intensity I_x by the total cross-sectional area of both the 6μm-wide Pt(3 nm) Hall channel and the 2μm-wide Co(0.5 nm)/Pt(2 nm) pillar. The duration of every pulse is 10 ms and the anomalous Hall resistance R_H was obtained by measuring the *y*-direction voltage under a small *x*-direction d.c. current (100 μA) 1 second after each pulse. To clarify the switching probability, the presented R_H data was normalized by the out-of-plane magnetic field (H_z)-induced maximum Hall resistance of each pillar.

All devices discussed in this article showed good PMA with similar magnetic anisotropy field (H_k) both before and after the localized laser annealing, as illustrated in Supplementary S1. The schematic drawing of a locally laser annealed device is shown in Figure 1a. Stacks of Pt(3 nm)/Co(0.5 nm)/Pt(2 nm) (from the substrate side) were deposited on Si/SiO_2 substrates by magnetron sputtering. After deposition, the stacks were processed into 6μm-wide Pt(3 nm) Hall bars with 2μm-wide Co(0.5 nm)/Pt(2 nm) square pillars on top of each pair of Hall contacts. A laser with wavelength of 532 nm and power of 8 mW was used to locally anneal each pillar by sweeping across it along the *x*-direction, leaving a localized laser annealing track on the -*y*/+*y* side of the left/right pillar. A sequence of 10 ms current pulses was applied with a varying current density J_x, where J_x was calculated by dividing the current intensity by the cross-sectional area of both the 6μm-wide Pt(3 nm) Hall channel and the 2μm-wide Co(0.5

nm)/Pt(2 nm) pillar. The perpendicular magnetization of each pillar was characterized by measuring the anomalous Hall resistance (R_H) using a small current of 100 μA following a 1 s interval after every pulse. As shown in Figure 1b and 1c, both locally laser annealed pillars showed 100% deterministic in-plane current-induced magnetization switching in the absence of external magnetic field, where the switching probability was given by the ratio of current-induced R_H to the maximum external magnetic field induced anomalous Hall resistance R_H^{max} (i.e. R_H/R_H^{max}) induced by an external out-of-plane magnetic field. Particularly, the sense of rotation of the J_x-induced switching loop is opposite between the -y side (anticlockwise switching) and the +y side annealed pillars (clockwise switching). This observed dependence of the switching sense on the location of the laser track could be exploited in integrated circuits with complementary spin logic and/or memory units[28,29].

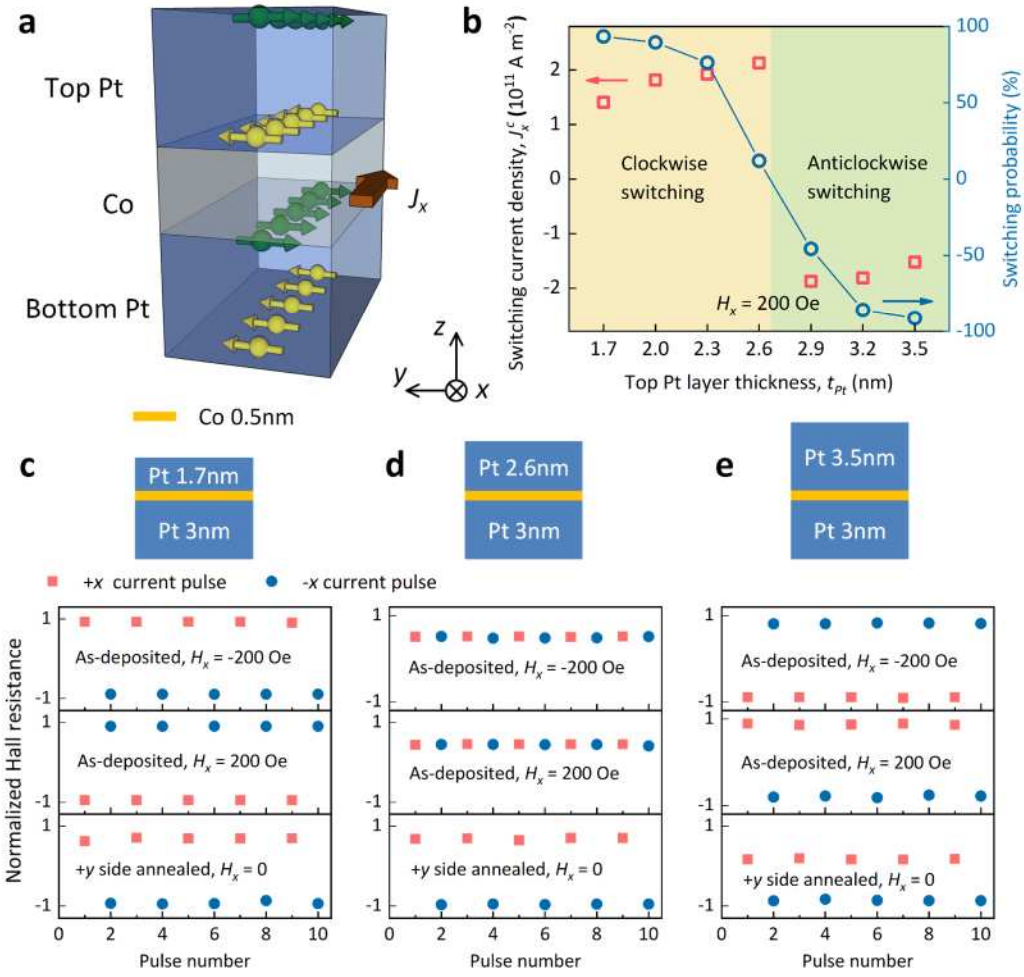

Figure 2 | Current-induced magnetization switching of as-deposited and locally laser annealed Pt(3 nm)/Co(0.5 nm)/Pt(t_{Pt}) trilayers. a, Schematic of spin current injection for positive J_x in a Pt/Co/Pt trilayer structure. The green and the yellow arrows represent spins polarized in the -y and the +y-directions, respectively. **b**, Critical switching current density (J_x^c, red squares, defined as the average of the values of J_x for magnetization switching from +z to -z directions) and switching probability (blue circles) versus t_{Pt} for as-deposited Pt(3 nm)/Co(0.5 nm)/Pt(t_{Pt}) samples. During the measurements, an in-plane magnetic field H_x = 200 Oe was applied.

Positive/negative J_x^c and switching probability denotes clockwise/anticlockwise switching, respectively. **c-e**, Magnetization switching with alternative positive and negative in-plane currents, for the as-deposited ($|J_x| = 2 \times 10^{11}$ A m^{-2}, $H_x = \pm 200$ Oe) and the +*y* side 16 mW locally laser annealed ($|J_x| = 2.8 \times 10^{11}$ A m^{-2}, without external magnetic field) samples with stack structures of (**c**) Pt(3 nm)/Co(0.5 nm)/Pt(1.7 nm), (**d**) Pt(3 nm)/Co(0.5 nm)/Pt(2.6 nm), and (**e**) Pt(3 nm)/Co(0.5 nm)/Pt(3.5 nm), respectively.

A series of Pt(3 nm)/Co(0.5 nm)/Pt(t_{Pt}) trilayers were deposited and fabricated into Hall bars (without pillars) to investigate the dependence of the magnetization switching on the out-of-plane spin current for both as-deposited samples and locally laser annealed samples. As illustrated in Figure 2a, spin currents with opposite polarization are injected into the Co layer from the bottom and the top Pt layers. The threshold for current-induced magnetization switching was determined in an in-plane external magnetic field $H_x = 200$ Oe. The critical switching current density J_x^c and the switching probability as functions of the top Pt layer thickness t_{Pt} for the as-deposited samples are shown in Figure 2b, where we defined the positive/negative J_x^c and switching probability (R_H/R_H^{max}) as representing the clockwise/anticlockwise switching respectively. The sense of rotation of the deterministic switching gradually evolves from clockwise to anticlockwise with growing t_{Pt}, indicating the injected spin

current is dominated by the bottom Pt layer for $t_{Pt} \leq 2.6$ nm and by the top Pt layer for $t_{Pt} \geq 2.9$ nm. For the approximately symmetric structure with t_{Pt} = 2.6 nm, the sample exhibits weak current-induced magnetization switching with a large J_x^c of 2.13×10^{11} A m^{-2} and a small switching probability of 11.9%. This indicates that the spin currents from the bottom and the top Pt layers are mostly neutralized.

A comparison of current pulse-induced magnetization switching behavior between the as-deposited and the locally laser annealed samples is shown in Figure 2c-e. For $J_x = \pm 2 \times 10^{11}$ A m^{-2} and $H_x = \pm 200$ Oe, no noticeable change in R_H was observed in the as-deposited Pt(3 nm)/Co(0.5 nm)/Pt(2.6 nm) sample while binary R_H with opposite signs were obtained in the as-deposited Pt(3 nm)/Co(0.5 nm)/Pt(1.7 nm) and Pt(3 nm)/Co(0.5 nm)/Pt(3.5 nm) samples. The sign of R_H depends on all the three aspects, namely, the sign of J_x, the sign of H_x, and the stack structure (i.e. t_{Pt} =1.7 nm in Figure 2c, or t_{Pt} = 3.5 nm in Figure 2e). However, the samples with t_{Pt} = 1.7 nm, 2.6 nm and 3.5 nm subjected to 16 mW localized laser annealing at the +y side of their Hall cross areas (drawn schematically in Supplementary Figure S1a) all showed substantial zero-field current-induced magnetization switching with the same switching sense regardless of the overall spin current polarization from the two Pt layers: the sign of R_H depends only on the sign of the electrical current (here $J_x = \pm 2.8 \times 10^{11}$ A m^{-2}) and the location of the laser track. These results suggest the

existence of a new, efficient, in-plane current-induced SOT with perpendicular effective magnetic field originating from the localized laser annealing, the direction of which is independent with the polarization of the injected spin current. In other words, current-induced magnetization switching without a net out-of-plane spin current injection can be realized in these locally laser annealed systems.

Furthermore, current-induced in-plane effective fields, which can be generated from an out-of-plane spin current injection, were also considered by conducting harmonic Hall measurements[12]. By analyzing the first and second harmonic signals of Pt(3 nm)/Co(0.5 nm)/Pt(2.6 nm) Hall bar samples (without pillar), as illustrated in Supplementary S2, no distinguishable damping-like torque can be determined for both the as-deposited and the 16 mW locally laser annealed samples. Out-of-plane spin current injections are thus once again shown, for both the as-deposited and the locally laser annealed sample, to be not strong enough to result in the current-induced magnetization switching. It further confirms that the current induced deterministic magnetization switching is coming from the localized laser annealing.

Spin-orbit torque due to lateral Pt-Co asymmetry

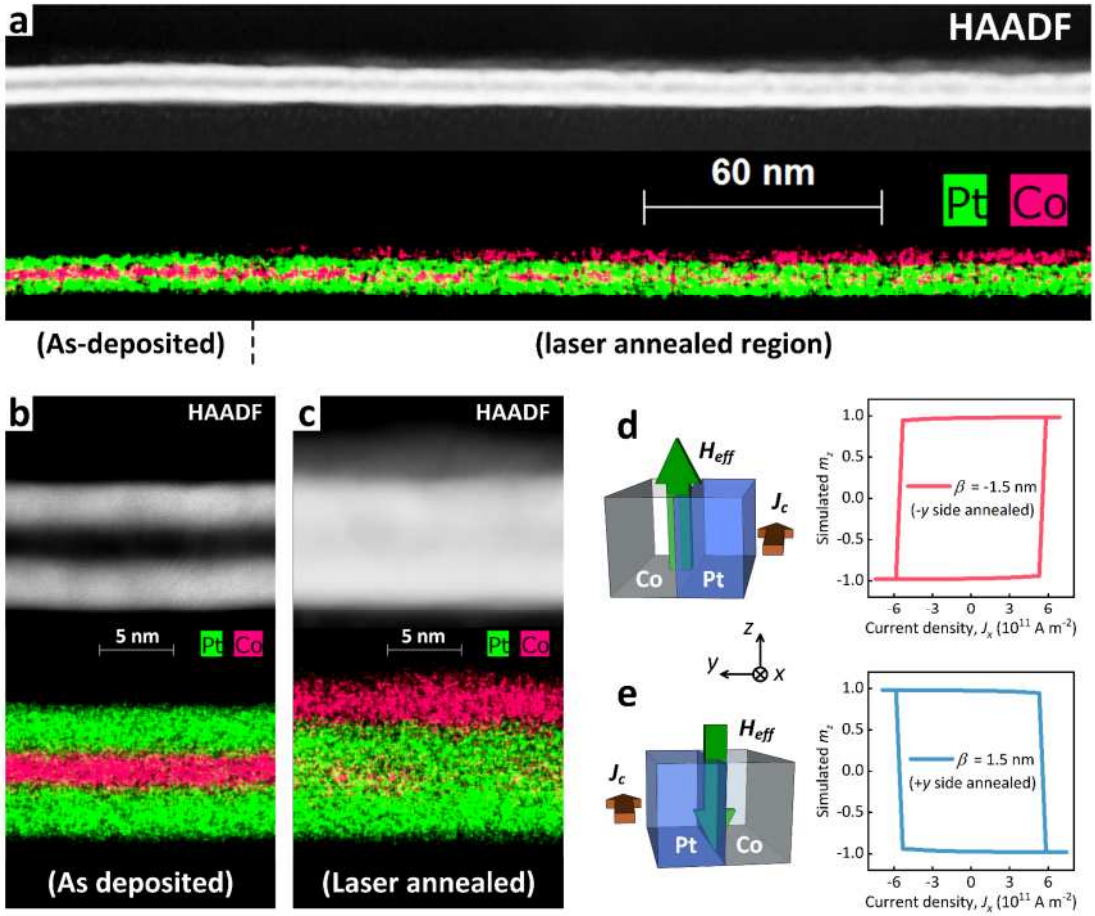

Figure 3 | Cross-sectional STEM observation of the locally laser annealed Pt/Co/Pt trilayer and micromagnetic simulation of the current-induced magnetization switching in lateral Pt-Co asymmetric thin films. Cross-sectional HAADF Z-contrast STEM images and corresponding EDS maps of a 12 mW locally laser annealed Pt(3 nm)/Co(3 nm)/Pt(3 nm) trilayer for (a) gradient area, (b) as-deposited region, and (c) laser annealed region, respectively. From bottom to top, there are the SiO_2 substrate surface, the Pt/Co/Pt trilayer, and the C capping layer. Brighter contrast corresponds to the heavier element (Pt) and darker contrast to the lighter elements (Co, Si, C). **d-e**, Simulated m_z-J_x loops with localized laser

annealing at (**d**) the -*y* side (Pt/Co interface in +*y*-direction, given β = -1.5 nm) and (**e**) the +*y* side (Pt/Co interface in -*y*-direction, given β = 1.5 nm), respectively. The micromagnetic simulation was performed using Mumax3.

In order to reveal the nature of the deterministic current-induced magnetization switching in the locally laser annealed Pt/Co/Pt devices, we acquired microscopic pictures of both the as-deposited and the laser annealed regions. A cross-sectional STEM sample was fabricated from a 12 mW locally laser annealed Pt(3 nm)/Co(3 nm)/Pt(3 nm) 6μm-wide Hall bar using a focused ion beam (FIB) instrument, followed by high-angle annular dark field (HAADF) STEM, bright field (BF) STEM, and X-ray energy-dispersive spectrometry (EDS) experiments. The HAADF image contrast scales with the square of the atomic number (*Z*), i.e. brighter contrast represents heavier element (Pt) and darker contrast represents lighter element (Co, Si, C). On the contrary, the BF images give complementary, inverse contrast, as shown in Supplementary S3. Figure 3a shows the HAADF Z-contrast image and the corresponding EDS mapping of the gradient area containing the as-deposited and the laser annealed regions. The two regions are shown on an expanded scale in Figure 3b and 3c respectively. Distinct Pt/Co/Pt layers can be observed in the as-deposited region, while the laser annealed region shows significant intermigration between the Co and the top Pt layers, resulting in a Pt/Co(t_1)/Pt/Co(t_2)-like structure with laterally varying Co components t_1

and t_2. Extended HAADF and BF images covering the whole laser annealed region are shown in Supplementary S3, confirming that the effective width of the 12 mW laser annealing track for the Pt(3 nm)/Co(3 nm)/Pt(3 nm) sample is around 660 nm. The average laser power per unit area in this case (laser power = 12 mW) is then estimated as about 2.75×10^{10} W m^{-2}. Since the intensity of a laser spot has a Gaussian distribution, there is no distinct boundary between the as-deposited and the laser annealed regions, and the ratio of t_2 to t_1 increases from the edge to the center of the laser annealed region. For a typical position near the center part of the laser annealed region, as shown in Figure 3c, most of the Co has migrated to the surface above the top Pt layers and is naturally oxidized into nonferromagnetic CoO_x[30,31].

The chemical composition gradient of Pt and Co elements results in a lateral interface between the laser annealed (mostly Pt) region and the as-deposited (Co) region. Analogous to the conventional SOT in perpendicularly asymmetric Pt/Co bilayers, the in-plane current J_x induces a new SOT acting on the as-deposited Co region due to the lateral Pt/Co interface, with a perpendicular effective field given by

$$H_z^{eff} = \beta \hat{y} \times J_x \quad (1).$$

The β coefficient of this SOT relates the magnitude of the effective field with the degree of the lateral Pt-Co asymmetry, which depends on the laser power. The sign of β depends on the relative location of the laser track,

given as positive if the track is on the $+y$ side of the device. As shown in Figure 3d and 3e, micromagnetic simulations of the m_z-J_x loops using an uniform magnetic film with given β = -/+ 1.5 nm were performed by MuMax3 using Equation (1),[32] the switching senses of which are in accordance with the experimental results in Figure 1b and 1c, respectively. Note that the generally demonstrated lateral SOT with a material-related coefficient β could be possibly explained by the lateral forms of spin Hall effect (where perpendicular polarized spins accumulate at the lateral Pt/Co interface) or equivalent Rashba effect or both, detailed mechanisms of which need further investigation. In any case, the inverted Co and upper Pt layers and the resulting lateral Pt-Co asymmetry are ascribed as the fundamental origin for the observed deterministic current-induced magnetization switching, which determines the magnitude and direction of the lateral SOT coefficient β.

Dependence of the current-induced H_z^{eff} on the laser power

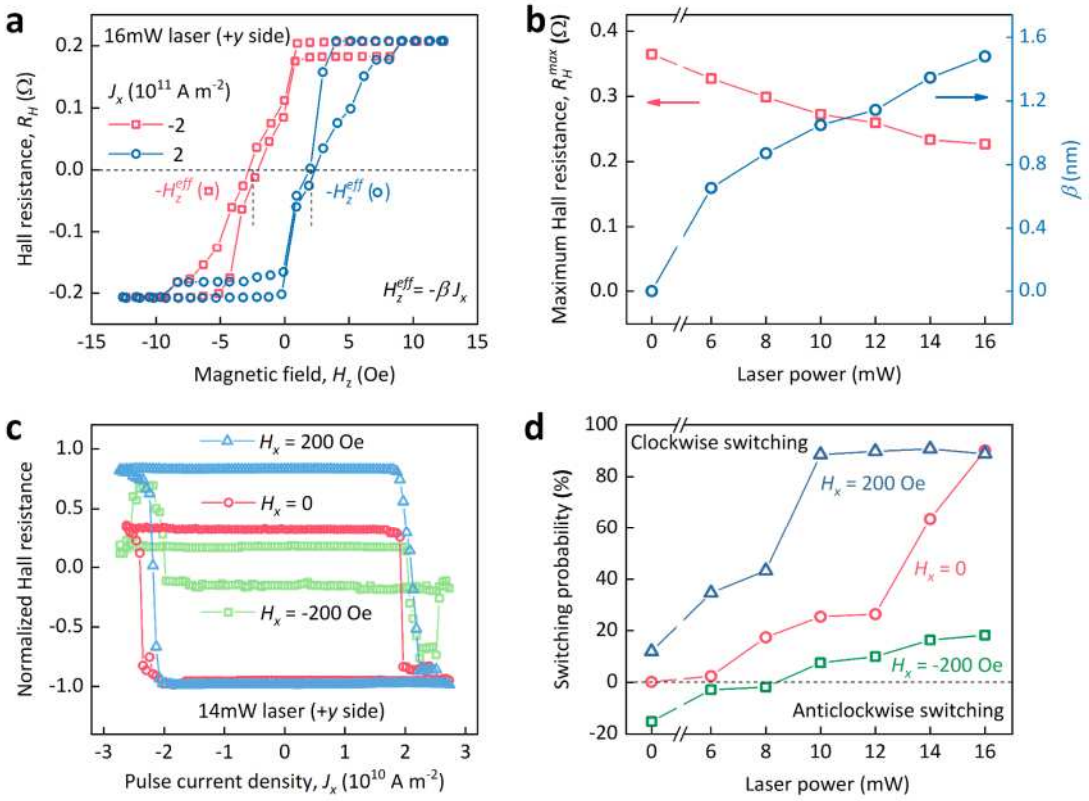

Figure 4 | Current-induced effective magnetic field and magnetization switching for locally laser annealed Pt(3 nm)/Co(0.5 nm)/Pt(2.6 nm) Hall bars with varying laser power. a, R_H-H_z loops of the 16 mW +y side locally laser annealed sample under constant d.c. currents of $J_x = \pm 2 \times 10^{11}$ A m^{-2}. The J_x-induced effective magnetic field H_z^{eff} was determined from each loop as the negative of its average coercivity field. **b**, The maximum Hall resistance R_H^{max} obtained in an external out-of-plane magnetic field (red squares) and the SOT coefficient β due to lateral Pt-Co asymmetry (defined as $\beta = -H_z^{eff}/J_x$, blue circles) versus laser power. **c**, Pulse current-induced R_H-J_x loops of the 14 mW +y side locally laser annealed sample with H_x = -200 Oe (green squares), H_x = 0 (red circles), and H_x = 200 Oe

(blue triangles), respectively. **d**, The current-induced magnetization switching probability as a function of the laser power with H_x = -200 Oe (green squares), H_x = 0 (red circles), and H_x = 200 Oe (blue triangles), respectively. The switching probability was obtained by dividing the J_x-induced maximum R_H by the external field-induced maximum R_H^{max}, where a positive/negative switching probability denotes a clockwise/anticlockwise switching.

To quantitatively determine β and further investigate its effect on the current-induced magnetization switching, R_H loops were measured versus external out-of-plane field under fixed *dc* currents, for Pt(3 nm)/Co(0.5 nm)/Pt(2.6 nm) samples with local laser annealing on the +*y* side. As shown in Figure 4a, the H_z^{eff} induced by a given J_x can be extracted from the R_H-H_z loop as its horizonal shift from zero point, where a left offset gives positive H_z^{eff} while a right shift gives negative H_z^{eff}. The β can thus be determined from $\beta = -H_z^{eff}/J_x$, a scalar form of Equation (1). The increase of β and reduction of maximum Hall resistance (R_H^{max}) with increasing laser power, as shown in Figure 4b and Supplementary S1, is in accordance with an increasing lateral Pt-Co asymmetry.

Pulsed current-induced magnetization switching loops with β = 1.35 nm (laser power = 14 mW) under various in-plane magnetic fields H_x are shown in Figure 4c. Switching probabilities, defined as the ratio of J_x-induced to external field-induced R_H^{max}, of 16.4%, 63.6%, and 90.8% were

obtained for H_x = -200 Oe, H_x = 0, and H_x = 200 Oe, respectively. Note that the observed unequal switching between H_x = -200 Oe and H_x = 200 Oe is quite different from the case in conventional SOT-induced magnetization switching. By comparing the switching probabilities for H_x = ±200 Oe and H_x = 0 as functions of the laser power, as shown in Figure 4d, we ascribe a joint effect of two independent mechanisms for nonzero-H_x-assisted current-induced magnetization switching: the conventional SOT from the perpendicular asymmetry, and the SOT from the localized laser annealing induced lateral Pt-Co asymmetry. Particularly, the zero-field switching probability gradually increases from 0% to 90.2% (regarded as an approximately full switching due to the considerable current shunting effect in a Hall bar device without pillars[33], see the switching loop in Supplementary S4) on increasing the laser power from 0 mW to 16 mW, owing to an increasing H_z^{eff} from the lateral Pt-Co asymmetry-induced SOT (also see Supplementary S5, where a spatially varying β from the lateral Pt/Co interface to the other side of the device was considered using micromagnetic simulations, which can explain the observed partial magnetization switching under weak laser annealing powers). Meanwhile, the anticlockwise switching with H_x = -200 Oe in the as-deposited sample converts into clockwise switching for samples with 10 mW and higher laser powers, indicating a competition between two H_z^{eff} with different signs. In contrast, the switching probability with H_x = 200 Oe, which is only 11.9%

for the as-deposited sample, increases rapidly to nearly full switching (88.6%) for 10 mW laser annealed samples (and maintains full switching for higher laser powers with a gradually decreasing J_x^c, as illustrated in Supplementary S6), indicating a constructive effect of two H_z^{eff} with the same sign. These results are consistent with the interplay of effective fields: the sign of conventional SOT-induced H_z^{eff} changes on reversing H_x, while the β-induced H_z^{eff} stays constant under different H_x. This further illustrates the SOT from lateral Pt-Co asymmetry as an important effect, independent of the external out-of-plane spin current, for deterministically switching a PMA-FM layer.

The technology of local laser annealing is promising for fabricating scalable spintronic devices. A similar case is the matured proposal of heat-assisted magnetic recording (HAMR)[34], where a locally laser induced thermal effect assists the magnetization switching of independent magnetic recording units within tens of nanometers, which is under intensive production development now[35]. Moreover, the fabrication of a lateral Pt-Co asymmetry may not be limited to our localized laser annealing method. Looking to the future, technologies capable of generating analogous lateral asymmetry inside a FM are expected to facilitate the current-induced magnetization switching without external out-of-plane spin current.

In summary, by introducing a lateral Pt gradient within the magnetic layer by localized laser annealing, an in-plane current-induced perpendicular effective magnetic field is generated which can deterministically switch the perpendicular magnetization at zero external magnetic field. The polarization and magnitude of the new SOT under an in-plane current depend only on the direction and degree of the lateral Pt-Co asymmetry, which are independent of the spin currents from neighboring layers or interfaces. The described lateral SOT offers a pathway to all electrical manipulation of spins without external out-of-plane spin current injection, and provides further insights into the in-plane current-induced SOTs in such asymmetric structures.

Experimental Section

Thin film preparation: The films were deposited at room temperature onto 0.5mm-thick Si wafers with a 190nm-thick thermal SiO_2 surface. D.C. magnetron sputtering was used to deposit the Pt and the Co layers. The base pressure of the chamber was less than 2×10^{-6} Pa, and Ar gas was used for sputtering. The pressure of the chamber was 1.064×10^{-1} Pa during deposition. No magnetic field was applied during the sputtering. The deposition rates for Pt and Co layers were controlled to be ~0.023 nm s^{-1} and ~0.012 nm s^{-1}, respectively.

Device fabrication: Two types of Hall bar devices were used in this work. For Hall bar devices with pillars, as shown in Figure 1, two steps of standard electron-beam lithography (EBL) and Ar ion etching were used. First, the Pt(3 nm)/Co(0.5 nm)/Pt(2 nm) film was patterned into a Hall bar with channel width of 6 μm. Then, the central areas of the Hall bar crosses were patterned into 2×2 μm^2 square pillars, leaving the rest of the Hall bar with only the bottom Pt(3 nm) layer; For Hall bar devices without pillars, used in Figure 2 and Figure 4, Pt(3 nm)/Co(0.5 nm)/Pt(t_{Pt}) films were used and all the three layers of each stack were patterned into a Hall bar with channel width of 6 μm.

Localized laser annealing: A laser with wavelength of 532 nm and power from 6 to 16 mW was used to locally anneal each sample in air atmosphere

by sweeping along the *x*-direction with a velocity of 0.167 μm/s. The sweeping was realized by fixing the laser spot position meanwhile controlling the position and movement of the sample using a three-dimensional automated stage and a Thorlabs APT piezo controller, with an in-plane resolution of 5 nm. The locations of the localized laser annealing tracks were controlled at either the -*y* or the +*y* side of the pillar (Figure 1) or the cross area of the Hall bar (Figures 2 and 4).

Estimation of the temperature raised by laser annealing: The diameter of the laser spot size is about 1.5 μm, however, the width of actual region affected by laser annealing depends on the local temperature distribution in the sample, which varies with the laser power, the sample structure, and sweeping speed of the laser. By annealing the Pt(3 nm)/Co(0.5 nm)/Pt(2.6 nm) films rapidly (9 seconds, the average retention time of the ~1.5 μm laser spot with a sweeping speed of 0.167 μm/s) with various temperature using a heat plate, fully nonferromagnetic samples were obtained after 350~400 □ annealing, which was estimated as the minimum laser-induced temperature rise for creating a significant lateral Pt-Co asymmetry such as the case shown in Figure 3c.

Measurement and characterization: The current-induced magnetization switching and anomalous Hall effect measurements were carried out at room temperature with a Keithley 2602B as the current source and Keithley

2182 as the nanovoltmeter. The Kerr imaging measurements were carried out using an Evico Kerr Microscope. The harmonic voltage measurements were conducted using two SR830 DSP lock-in amplifiers. The sample for STEM characterization was prepared using a Zeiss Auriga FIB system. The HAADF Z-contrast images, the BF images, and the EDS mappings were acquired on a spherical aberration-corrected FEI Titan Cubed Themis 60-300 operated at 200 kV.

Calculation of the current density: There should be different conductive cross sectional areas between devices before and after the localized laser annealing due to oxidation of the migrated Co. Hence the current densities used in this study, which are calculated by dividing the current intensity with the whole pristine Pt/Co/Pt cross section area, should be regarded as approximate values for clarity.

Supporting Information

Supplementary Information is available from the Wiley Online Library or from the authors.

Acknowledgements:

This work was supported by National Key R&D Program of China (Grant No. 2017YFB0405700), by the NSFC (Grant No. 11474272 and

61774144), by Chinese Academy of Sciences (Grant No. QYZDY-SSW-JSC020, XDPB12, and XDB28000000), and by Beijing Natural Science Foundation Key Program (Grant No. Z190007).

Competing Interests

The authors declare no competing financial interests.

Additional Information

Correspondence and requests for materials should be addressed to K.W.

References

1. Y. M. Huai, *AAPPS Bulletin* **2008**, *18*, 33.

2. S. S. P. Parkin, M. Hayshi, L. Thomas, *Science* **2008**, *320*, 190.

3. I. M. Miron, K. Garello, G. Gaudin, P.-J. Zermatten, M. V. Costache, S. Auffret, S. Bandiera, B. Rodmacq, A. Schuhl, P. Gambardella, *Nature* **2011**, *476*, 189.

4. L. Liu, C. F. Pai, Y. Li, H. W. Tseng, D. C. Ralph, R. A. Buhrman, *Science* **2012,** *336*, 555.

5. Z. Luo, T. P. Dao, A. Hrabec, J. Vijayakumar, A. Kleibert, M. Baumgartner, E. Kirk, J. Cui, T. Savchenko, G. Krishnaswamy, L. J. Heyderman, P. Gambardella, *Science* **2019**, *363*, 1435.

6. N. Locatelli, V. Cros, J. Grollier, *Nat. Mater.* **2014**, *13*, 11.

7. S. Fukami, T. Anekawa, C. Zhang, H. Ohno, *Nat. Nanotechnol.* **2016**, *11*, 621.

8. Y. Li, K. W. Edmonds, X. Liu, H. Zheng, K. Wang, *Adv. Quantum Technol.* **2019**, *2*, 1800052.

9. A. Brataas, A. D. Kent, H. Ohno, *Nature Mater.* **2012**, *11*, 372.

10. I. M. Miron, G. Gaudin, S. Auffret, B. Rodmacq, A. Schuhl, S. Pizzini, J. Vogel, P. Gambardella, *Nature Mater.* **2010**, *9*, 230.

11. L. Liu, O. J. Lee, T. J. Gudmundsen, D. C. Ralph, R. A. Buhrman,

Phys. Rev. Lett. **2012**, *109*, 96602.

12. M. Yang, K. Cai, H. Ju, K. W. Edmonds, G. Yang, S. Liu, B. Li, B. Zhang, Y. Sheng, S. Wang, Y. Ji, K. Wang, *Sci. Rep.* **2016,** *6*, 20778.
13. V. P. Amin, J. Zemen, M. D. Stiles, *Phys. Rev. Lett.* **2018**, *121*, 136805.
14. K. Cai, M. Yang, H. Ju, S. Wang, Y. Ji, B. Li, K. W. Edmonds, Y. Sheng, B. Zhang, N. Zhang, S. Liu, H. Zheng, K. Wang, *Nat. Mater.* **2017**, *16*, 712.
15. M. Yang, Y. Deng, Z. Wu, K. Cai, K. W. Edmonds, Y. Li, Y. Sheng, S. Wang, Y. Cui, J. Luo, Y. Ji, H. Zheng, K. Wang, *IEEE Electron. Dev. Lett.* **2019**, *40*, 1554.
16. M. Yang, Y. Deng, K. Cai, H. Ju, S. Liu, B. Li, K. Wang, *J. Mang. Magn. Mater.* **2019**, *489*, 165474.
17. G. Yu, P. Upadhyaya, Y. Fan, J. G. Alzate, W. Jiang, K. L. Wong, S. Takei, S. A. Bender, L. Chang, Y. Jiang, M. Lang, J. Tang, Y. Wang, Y. Tserkovnyak, P. K. Amiri, K. L. Wang, *Nat. Nanotech.* **2014**, *9*, 548.
18. L. You, O. Lee, D. Bhowmik, D. Labanowski, J. Hong, J. Bokor, S. Salahuddin, *Proc. Natl. Acad. Sci.* **2015,** *112*, 10310.
19. S. Fukami, C. Zhang, S. DuttaGupta, A. Kurenkov, H. Ohno, *Nat.*

Mater. **2016,** *15*, 535.

20. Y. W. Oh, S. C. Baek, Y. M. Kim, H. Y. Lee, K. D. Lee, C. G. Yang, E.S. Park, K. S. Lee, K. W. Kim, G. Go, J. R. Jeong, B. C. Min, H. W. Lee, K. J. Lee, B. G. Park, *Nat. Nanotech.* **2016**, *11*, 878.

21. Y.-C. Lau, D. Betto, K. Rode, J. Coey, P. Stamenov, *Nat. Nanotechnol.* **2016,** *11*, 758.

22. Y. Sheng, K. W. Edmonds, X. Ma, H. Zheng, K. Wang, *Adv. Electron. Mater.* **2018,** *4*, 1800224.

23. Y. Cao, A. W. Rushforth, Y. Sheng, H. Zheng, K. Wang, *Adv. Funct. Mater.* **2019**, *29*, 1808104.

24. N. Sato, F. Xue, R. M. White, C. Bi, S. Wang, *Nat. Electron.* **2018**, *1*, 508.

25. M. Wang, W. Cai, D. Zhu, Z. Wang, J. Kan, Z. Zhao, K. Cao, Z. Wang, Y. Zhang, T. Zhang, C. Park, J.-P. Wang, A. Fert, W. Zhao, *Nat. Electron.* **2018**, *1*, 582.

26. S. C. Baek, V. P. Amin, Y.-W. Oh, G. Go, S.-J. Lee, G.-H. Lee, K.-J. Kim, M. D. Stiles, B.-G. Park, K.-J. Lee, *Nat. Mater.* **2018**, *17*, 509.

27. D. MacNeill, G. M. Stiehl, M. H. D. Guimaraes, R. A. Buhrman, J. Park, D. C. Ralph, *Nat. Phys.* **2016**, *13*, 300.

28. K. Wang, *Nat. Electron.* **2018**, *1*, 378.

29. S. C. Baek, K.-W. Park, D.-S. Kil, Y. Jang, J. Park, K.-J. Lee, B.-G. Park, *Nat. Electron.* **2018**, *1*, 398.

30. Y. Hibino, T. Hirai, K. Hasegawa, T. Koyama, D. Chiba, *Appl. Phys. Lett.* **2017**, *111*, 132404.

31. K. Hasegawa, Y. Hibino, M. Suzuki, T. Koyama, D. Chiba, *Phys. Rev. B* **2018**, *98*, 020405.

32. A. Vansteenkiste, J. Leliaert, M. Dvornik, M. Helsen, F. Garcia-Sanchez, B. V. Waeyenberge, *AIP Adv.* **2014**, *4*, 107133.

33. A. V. D. Brink, G. Vermijs, A. Solignac, J. Koo, J. T. Kohlhepp, H. J. M. Swagten, B. Koopmans, *Nat. Commun.* **2016**, *7*, 10854.

34. M. H. Kryder, E. C. Gage, T. W. McDaniel, W. A. Challener, R. E. Rottmayer, G. Ju, Y.-T. Hsia, M. F. Erden, *Proceedings of the IEEE*, **2008**, *96*, 1810.

35. M. T. Kief and R. H. Victora, *MRS Bull.* **2018**, *43*, 87.

Supplementary Information

Deterministic magnetization switching using lateral spin-orbit torque

*Yi Cao†, Yu Sheng†, Kevin William Edmonds, Yang Ji, Houzhi Zheng, and Kaiyou Wang**

Dr. Y. Cao, Y. Sheng, Prof. Y. Ji, Prof. H. Zheng, Prof. K. Wang
State Key Laboratory for Superlattices and Microstructures
Institute of Semiconductors
Chinese Academy of Sciences
Beijing 100083, China
E-mail: kywang@semi.ac.cn

Dr. Y. Cao, Prof. K. Wang
Beijing Academy of Quantum Information Sciences
Beijing 100193, China

Prof. K. W. Edmonds
School of Physics and Astronomy
University of Nottingham
Nottingham NG7 2RD, United Kingdom

Prof. Y. Ji, Prof. H. Zheng, Prof. K. Wang
Center of Materials Science and Optoelectronic Engineering
University of Chinese Academy of Science
Beijing 100049, China

Prof. K. Wang
Center for Excellence in Topological Quantum Computation
University of Chinese Academy of Science
Beijing 100049, China

†These authors contributed equally to this work.

*Corresponding e-mail: kywang@semi.ac.cn

Contents

S1. Magnetic properties of the Pt(3 nm)/Co(0.5 nm)/Pt(t_{Pt}) stacks before and after localized laser annealing

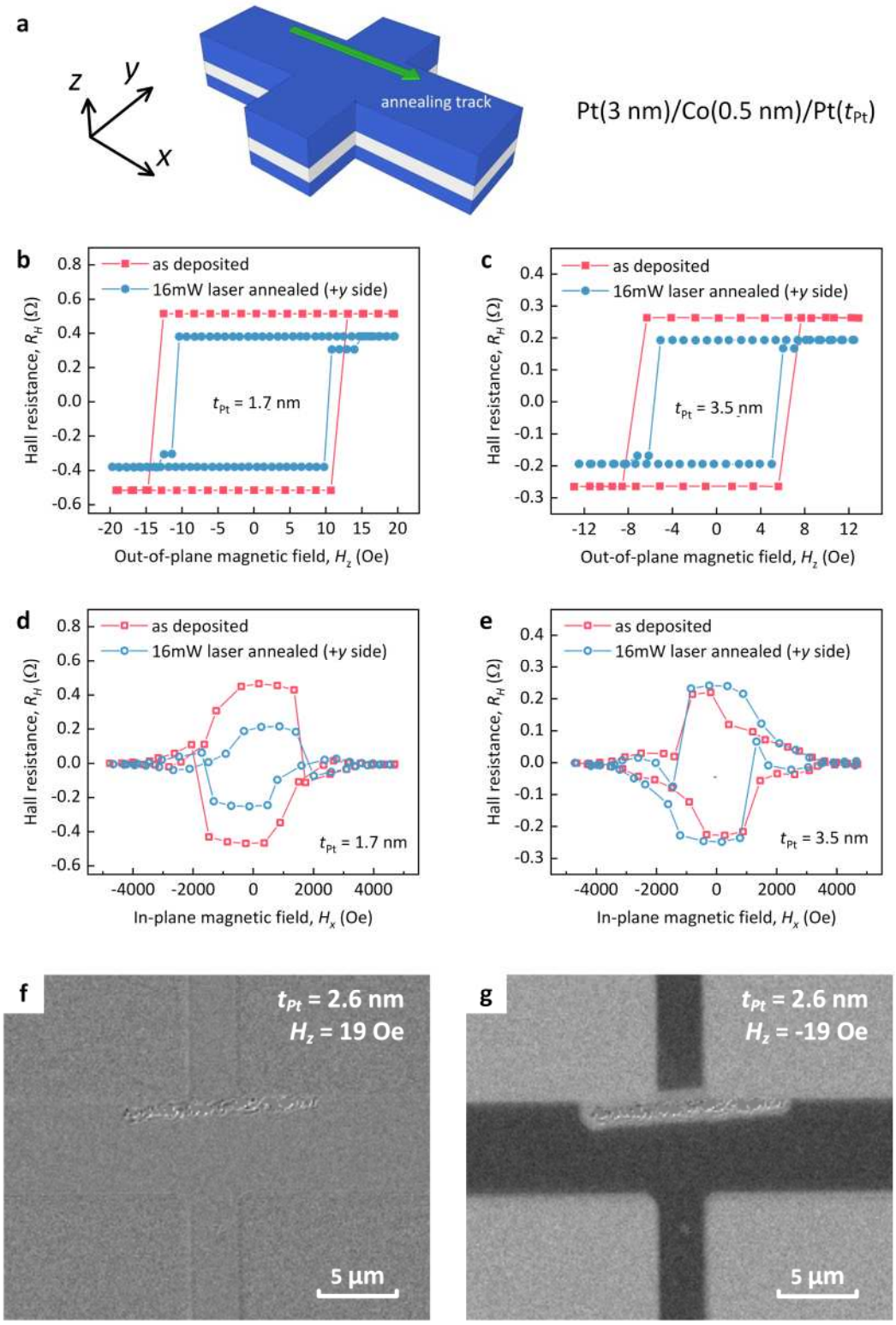

Figure S1 | Schematic drawing of the laser annealing location and

magnetic property changes of the stacks. a, Schematic drawing of the laser track location for a Hall bar device. **b-e**, (**b-c**) Out-of-plane magnetic field-induced R_H-H_z loops and (**d-e**) in-plane magnetic field-induced R_H-H_x loops for the as deposited (red squares) and the +*y* side 16 mW locally laser annealed (blue circles) samples with stack structures of (**b, d**) Pt(3 nm)/Co(0.5 nm)/Pt(1.7 nm) and (**c, e**) Pt(3 nm)/Co(0.5 nm)/Pt(3.5 nm), respectively. **f-g**, Polar Kerr microscopy images of the 16 mW locally laser annealed Pt(3 nm)/Co(0.5 nm)/Pt(2.6 nm) sample under (**f**) H_z = 19 Oe and (**g**) H_z = -19 Oe, respectively.

All the stack structures used in this article are Si/SiO_2 substrate/Pt(3 nm)/Co(0.5 nm)/Pt(t_{Pt}), where the top Pt layer t_{Pt} ranges from 1.7 nm to 3.5 nm. By measuring the R_H-H_z loops for samples with t_{Pt} = 1.7 nm and t_{Pt} = 3.5 nm, for representatives, the magnetic properties before and after the 16 mW localized laser annealing were examined. As shown in Figure S1b and S1c, both as deposited samples exhibit rectangle out-of-plane magnetic hysteresis loop, meanwhile, the hysteresis loops for 16 mW locally laser annealed samples keep good rectangularity but appear small jumps before reaching full magnetization switching. The small jumps in the hysteresis loops are supposed to be caused by the annealing track-induced pinning/blocking effect on the domain wall motions in the Hall crosses. Furthermore, the magnetic anisotropy field H_k (i.e. the in-plane magnetic field required for rotating a PMA moment to in-plane direction) were

determined to be around 3500 Oe for both samples whenever before or after the localized laser annealing, as shown by the in-plane magnetic field-induced R_H-H_x loops in Figure S1d and S1e, suggesting good PMA with roughly the same H_k for all the samples studied in this article, regardless of the top Pt thicknesses and the localized laser annealing.

Note that there is a reduction of the maximum Hall resistance R_H^{max} for both samples after the localized laser annealing. With the annealing induced relative displacement between Co and top Pt layers, changes of perpendicular saturation magnetization (which can be diminished to zero, when all the Co atoms moves above the top Pt layer and get oxidized) and/or interface condition in the laser annealed region are supposed to be responsible for this variation of anomalous Hall effect[1]. This assumption was supported by polar Kerr images of the 16 mW localized laser annealed Pt(3 nm)/Co(0.5 nm)/Pt(2.6 nm) sample with opposite H_z = ±19 Oe, as shown in Figure S1f and S1g, where a non-PMA strip with the width of 2.1 μm was found after the localized laser annealing. Following this way, the monotonically decreasing R_H^{max} shown in Figure 4b can be interpreted as a continuous enhancement of the lateral Pt-Co asymmetry in the device with the increasement of laser power. For simplification, the non-PMA strip width in Pt(3 nm)/Co(0.5 nm)/Pt(2.6 nm) samples created by laser power of 6 mW, 8 mW, 10 mW, 12 mW, and 14 mW are roughly estimated to be 0.6 μm, 1 μm, 1.4 μm, 1.6 μm, and 2 μm, respectively, by comparing

each R_H^{max} with the case of 16 mW (whose R_H^{max} = 0.227 Ω and non-PMA strip width = 2.1 μm). According to the STEM images and EDS mappings in Figure 3 as well as Figure S3, where most Co atoms of the laser affected region have immigrated to the surface of the film, nonferromagnetic CoO_x is believed to be the main constituents of the non-PMA strip.

S2. Harmonic measurement of the in-plane effective magnetic field

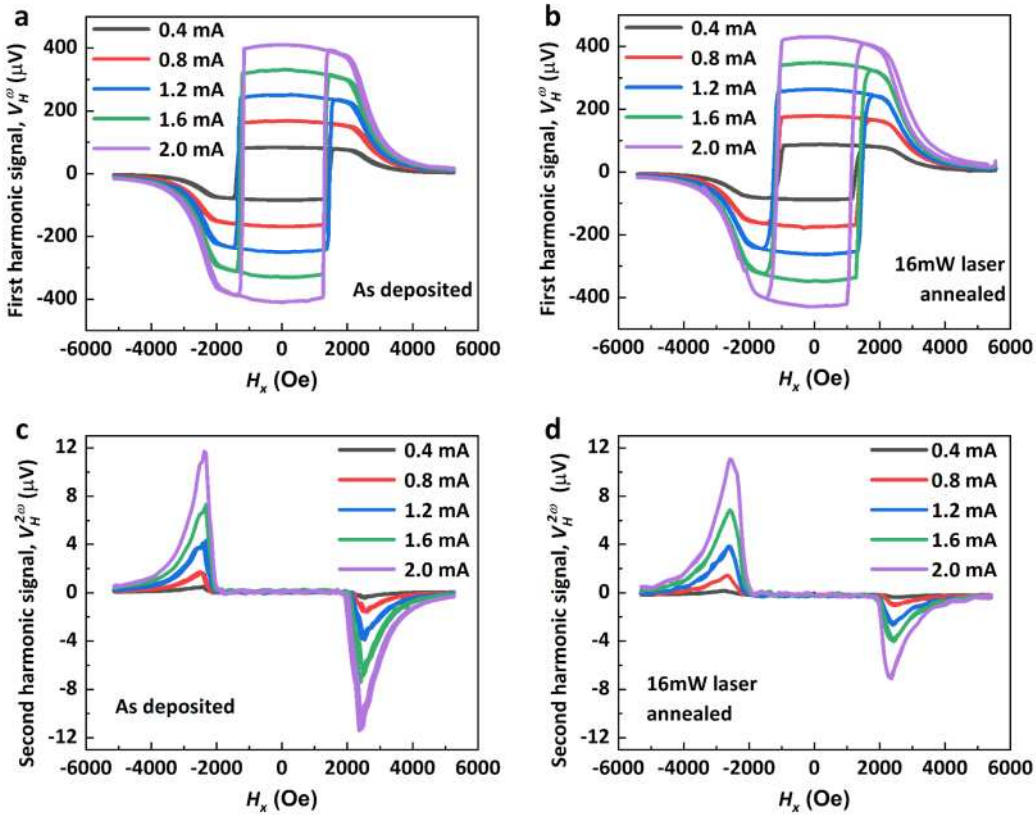

Figure S2 | First (a, b) and second (c, d) harmonic measurement of the as deposited (a, c) and the +*y* side 16 mW locally annealed (b, d) Pt(3

nm)/Co(0.5 nm)/Pt(2.6 nm) Hall bars (without pillars). A.C. current with magnitudes from 0.4 to 2.0 mA were applied to the channel along *x* direction, while first and second order Hall voltages were measured across the Hall arm in *y* direction. The scanning in-plane magnetic field was applied parallel to the *x* direction. The harmonic voltage measurements were conducted using two SR830 DSP lock-in amplifiers.

Harmonic measurements provide a powerful probe of the current-induced in-plane effective fields from the damping-like and the field-like torques. As illustrated in our previous work (manuscript Ref. 12), pillared Pt/Co/Pt device gives negligible field-like torque but significant damping-like torque with obviously tilted second harmonic Hall curve near $H_x = 0$. In the case of the as deposited Pt(3 nm)/Co(0.5 nm)/Pt(2.6 nm) Hall bars without pillar, however, almost flat and unchanged second harmonic signal curves were observed near $H_x = 0$ for the as-deposited and the 16 mW laser annealed samples with various applying a.c. channel current, as shown in Figure S2c and S2d. Although the peaks shape of second harmonic Hall signals show there are damping-like torque with same directions before and after the localized laser annealing[2], but the flat slopes of them near $H_x = 0$ suggest small values of the damping-like torques. This result agrees with the largely cancelled out-of-plane spin current injections from the bottom by the top Pt layers, but the value of which is small and remained nearly unchanged after localized laser annealing.

S3. HAADF and BF images of the locally laser annealed Pt/Co/Pt sample

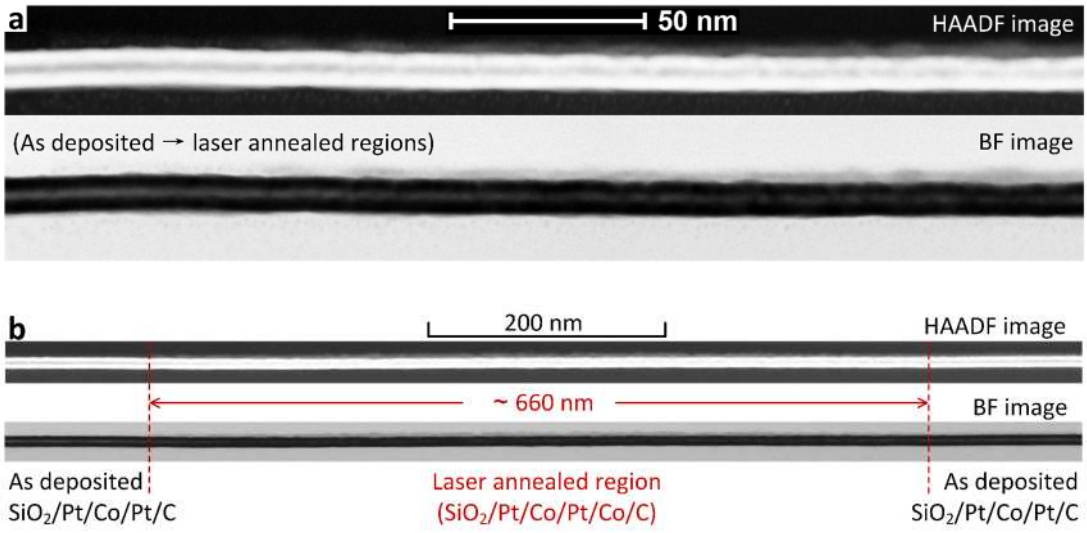

Figure S3 | HAADF and BF images of the 12 mW locally laser annealed SiO_2 substrate surface/Pt(3 nm)/Co(3 nm)/Pt(3 nm)/C capping layer STEM sample. Brighter contrast represents heavier (Pt) / lighter (Co, Si, and C) elements in the HAADF / the BF images, respectively. **a**, HAADF and BF images of the gradient area from the left as deposited to the right laser annealed regions. **b**, Extended HAADF and BF images covering the whole 12 mW laser annealed region. The boundaries between the as deposited and the laser annealed regions are defined at positions where distinguishable Co-Pt intermigration appears. Magnify the figure to see details.

The contrast in a BF image is inverse to a HAADF image, thus providing a complementary view to the macrostructure. A comparison in the BF and the HAADF images of the same area with Figure 3a is shown

in Figure S3a, where we can find that as deposited middle Co layer and the laser annealing-induced migrated top Co layer are more obvious in the HAADF image and the BF image, respectively.

Figure S3b shows extended HAADF and BF images covering the whole laser annealed region. By defining the boundary of the as-deposited and the laser annealed regions at the position where distinguished Co-Pt intermigration appears, the total width of the 12 mW laser annealed region for the Pt(3 nm)/Co(3 nm)/Pt(3 nm) sample was obtained as around 660 nm. Note that this value is apparently smaller than the estimated laser annealed strip width (1.6 μm) of the Pt(3 nm)/Co(0.5 nm)/Pt(2.6 nm) sample under a same 12 mW laser, where the film thickness is supposed to be a crucial factor for the heat dissipation condition and the resulting laser induced temperature rise. Moreover, the specific thickness of the upper Pt layer is also important since it determines the migration distance of the Co atoms (from the as-deposited Co layer to the surface of the film). For samples with thicker upper Pt layer, such as the Pt(3 nm)/Co(0.5 nm)/Pt(3.5 nm) sample shown in Figure 2e, there might be wider “Pt-Co gradient regions” and more complex magnetic and spin-orbit configurations, where the detailed effect on the lateral SOT induced magnetization switching requires further investigation.

S4. Zero-field R_H-J_x loop for the 16 mW locally laser annealed sample

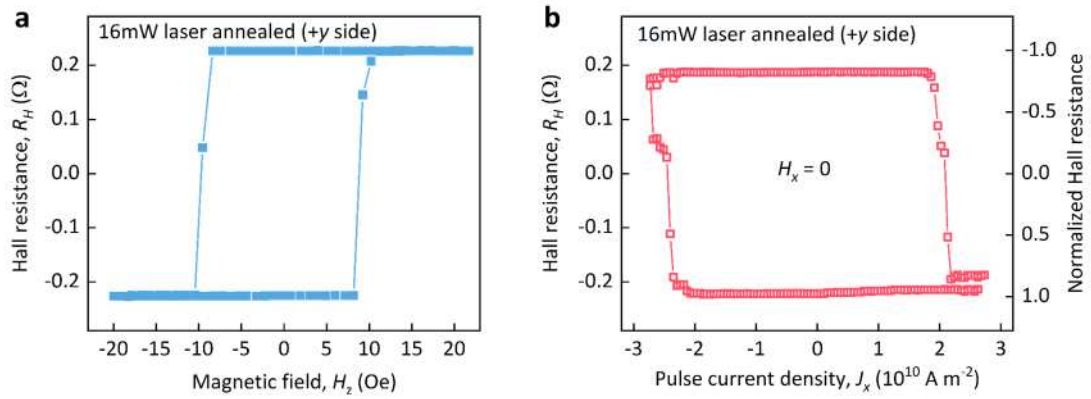

Figure S4 | The magnetic field-induced and the zero-field current-induced magnetization switching after localized laser annealing. a-b, (**a**) The R_H-H_z loop and (**b**) the zero-field R_H-J_x loop for the +*y* side 16 mW locally laser annealed Pt(3 nm)/Co(0.5 nm)/Pt(2.6 nm) Hall bar. The initial magnetic state was set fully downwards by H_z = -200 Oe before the current-induced magnetization switching measurement.

The out-of-plane magnetic field-induced as well as the zero-field current-induced magnetization switching loop of the +*y* side 16 mW locally laser annealed Pt(3 nm)/Co(0.5 nm)/Pt(2.6 nm) Hall bar device are shown in Figure S4a and Figure S4b, respectively. Considering the unneglectable current shunting effect in a Hall bar device without pillars, the measured Hall resistance R_H is not only contributed by the central cross area of the Hall bar, but also partly from the arms. Therefore, even a full magnetization switching is realized in the cross area, it is not possible for the measured R_H to reach the H_z-induced maximum Hall resistance R_H^{max}. In this way,

we regard the switching probability of ~90% in Figure 4d and Figure S4b as an approximately full current-induced magnetization switching.

S5. Simulation of the current-induced magnetization switching with spatially varying β

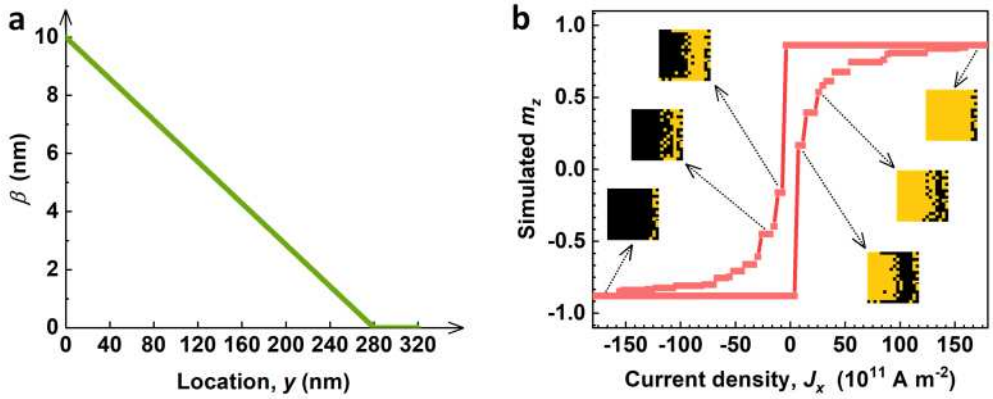

Figure S5 | Mumax3 micromagnetic simulation using spatially decreasing β. a, The given distribution of β along the y direction of a 320 nm × 320 nm Co (1nm) layer. **b**, Simulated m_z-J_x loop and corresponding domain distributions (yellow/black area denotes the spin up/down state) during the magnetization switching process.

From consideration of the lateral variation of the Co intermigration shown in Fig. 3a, the material-related lateral SOT coefficient β is expected to decrease from the lateral Pt/Co interface to the other side of the device. Following this reasonable assumption, current-induced magnetization switching was simulated again based on a linearly decaying β shown in

Figure S5a. The resulted m_z-J_x loop and corresponding domain distribution variations are shown in Figure 5b. The current-induced magnetization switching was shown to be achieved by domain wall motions from the left side (with larger β) to the right side (with smaller β) of the Co layer. Firstly, over half of m_z was rapidly switched at around $\pm 7 \times 10^{11}$ A m^{-2}. Then, the switching became a slow and gradient process before it reached about 88% of m_z (corresponding to the region of y < 280 nm shown in Figure S5a) at around $\pm 160 \times 10^{11}$ A m^{-2}, which could exceed the maximum safe current limit for a PMA Pt/Co/Pt device. Moreover, even though a sufficient current density was applied on the sample without destroying the magnetization or resistance, the creeping magnetization switching shown in Figure S5b could hardly happen when considering the pinning effect in real materials. Therefore, for samples with weak β (whose actual value of β may be much smaller at the location far from the lateral Pt/Co interface) there should be partial current-induced magnetization switching, such as the cases with laser power ≤ 14 mW shown in Figure 4d.

S6. J_x^c under H_x = 200 Oe for laser powers above 10 mW

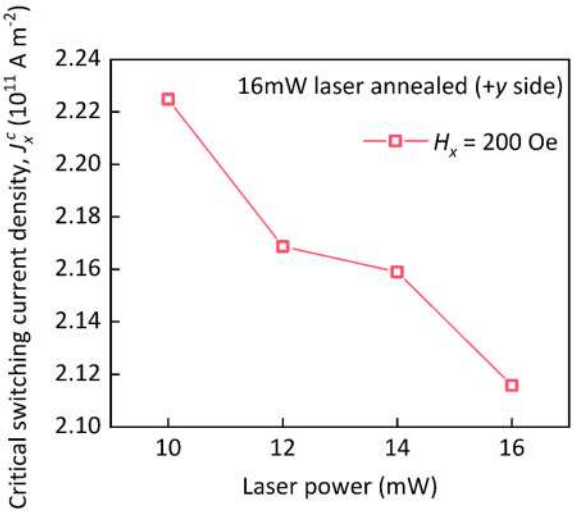

Figure S6 | In-plane magnetic field-assisted critical switching current density as a function of the laser power. The samples are Pt(3 nm)/Co(0.5 nm)/Pt(2.6 nm) Hall bar devices with localized laser annealing at the +y side. The assistant in-plane magnetic field H_x is fixed at 200 Oe and the laser powers ranges from 10 mW to 16 mW.

The critical current density J_x^c in this article is defined as the average values of J_x for the magnetization switching from +z to -z directions[3]. The J_x^c is usually used to evaluate the level of difficulty for a current-induced magnetization switching, however, for the cases in Figure 4d, where most of the switching probabilities are below 50%, the switching probability should be a more important indicator rather than the J_x^c.

For laser powers above 10 mW in Figure 4d, whose current-induced magnetization switching probabilities are all around 90% with the assistance of H_x = 200 Oe, their J_x^c were then considered for estimating

the switching difficulties. As shown in Figure S6, the J_x^c slightly decreases as the laser power increases from 10 mW to 16 mW, corresponding to enhanced current-induced perpendicular effective magnetic fields H_z^{eff} due to stronger lateral Pt-Co asymmetries with the growing laser power.

References

1. N. Nagaosa, J. Sinova, S. Onoda, A. H. MacDonald, N. P. Ong, *Rev. Mod. Phys.* **2010**, *82*, 1539.

2. X. Qiu, K. Narayanapillai, Y. Wu, P. Deorani, D.-H. Yang, W.-S. Noh, J.-H. Park, K.-J. Lee, H.-W. Lee, H. Yang, *Nat. Nanotechnol.* **2015**, *10*, 333.

3. S. Fukami, T. Anekawa, C. Zhang, H. Ohno, *Nat. Nanotechnol.* **2016**, *11*, 621.